scientific reports

Check for updates

OPEN

Spectroscopic approach to optimize the biogenic silver nanoparticles for photocatalytic removal of ternary dye mixture and ecotoxicological impact of treated wastewater

Keya Mandal[1,5], Dipti Das[1,5], Supriya Kumar Bose[1], Aparna Chaudhuri[1], Arpita Chakraborty[1], Sapna Mandal[1], Sabyasachi Ghosh[1,2,3]✉ & Swarup Roy[4]✉

The fabricating of extremely effective, economical, ecologically safe, and reusable nanoparticle (NP) catalysts for the removal of water pollution is urgently needed. This study, spectroscopically optimizes the process parameters for the biogenic synthesis of AgNP catalysts using *Cledrdendrum infortunatum* leaf extract. The optimization of several synthesis parameters was systematically studied using UV–Vis spectroscopy to identify the ideal conditions for AgNPs formation. The AgNPs are spherical with a size of ~ 20 nm, pure and stable. Mechanistic insights into the biogenic synthesis process were explored. The photocatalytic performance of biogenic AgNPs was evaluated for the degradation of three common (crystal violet, thioflavin T, and methylene blue) dyes as models in ternary mixtures under the influence of sunlight. AgNPs show excellent photocatalytic efficiency in terms of degradation percentage (82.89–96.96% within 110 min), kinetics (0.0247–0.0331 min^{-1}), half-life (20.96–28.11 min), and T_{80} (48.67–65.28 min) and also easily recovered and reused. Ecological safety assessment of the treated wastewater was assessed on the growths of rice, mustard, and lentil plants, and preliminary findings demonstrated that seedling growths for treated wastewater were nearly similar to the control sample but retarded in dye-contaminated wastewater suggesting potential use of treated wastewater for sustainable agriculture without compromising ecological balance. So, this study explores biogenic AgNPs as cost-effective, safe, and sustainable photocatalytic agents for the remediation of hazardous mix dyes and real-life applications of treated water for agricultural purposes.

Keywords Biosynthesis, Nanoparticles, Spectroscopy, Photocatalytic activity, Ecotoxicology

The escalating environmental pollution due to industrial effluents, particularly from dye and textile industries, poses a significant threat to ecosystems and human health[1–3]. Wastewater containing synthetic dyes, such as methylene blue (MB), thioflavin T (TT), and crystal violet (CV) are a serious health and environmental concern if they were discharged as a partially or untreated form of dyes[4–6]. Conventional wastewater treatment methods often fall short of effectively degrading these complex dye molecules[6,7], necessitating the development of more efficient and sustainable solutions. Nanotechnology, particularly the use of silver nanoparticles (AgNPs)[8] has emerged as a promising approach for addressing these challenges due to their unique physicochemical properties[9] and enhanced catalytic activities. Since ancient times Ag has been extensively used in water storage, food storage, and wound healing due to their intrinsic antimicrobial properties[10]. However, some publications

[1]Department of Biotechnology, School of Life Science, Swami Vivekananda University, Barrackpore, West Bengal 700121, India. [2]Department of Biochemistry and Biophysics, University of Kalyani, Nadia, Kalyani, West Bengal 741235, India. [3]Department of Agricultural Chemicals, Bidhan Chandra Krishi Viswavidyalaya, Nadia, Mohanpur, West Bengal 741252, India. [4]Department of Food Technology and Nutrition, School of Agriculture, Lovely Professional University, Phagwara 144411, India. [5]Keya Mandal and Dipti Das equally contributed to this work. ✉email: sghosh.id@gmail.com; swaruproy2013@gmail.com

raise concerns regarding acute toxicity because of the production of harmful metabolites, even after the complete degradation of dyes[11,12].

In particular, the plant extract-based biosynthesis method is presently under exploitation due to its simple, single-step, unique, non-toxic, faster, economical, non-pathogenicity, sustainable, and suitable for large-scale production. Plant extract comprises an enormous source of secondary metabolites including flavonoids, alkaloids, steroids, phenols, and terpenoids, which are responsible for reducing and stabilizing agents for biosynthesis of NPs[13,14]. Moreover, such bioactive phytochemicals are safer for the environment and even though the plant-based biosynthesis method improved stability. It requires a simple laboratory setup, is safe to handle, and provides flexibility in reaction parameters compared to other synthesis methods of NPs[15,16]. Among various plants, *Clerodendrum infortunatum* (Linn.) has been recognized for its strong phytochemical characteristics[17], and making it an ideal candidate for the biosynthesis of AgNPs. It is a versatile tree with extremely active biological components (secondary metabolites including flavonoids, triterpenes, and steroids) in its bark, leaves, seed extracts, and isolated parts[18,19]. Therefore, these properties of *C. infortunatum* (Linn.) motivated us to utilize the aqueous leaf extract for the biogenic synthesis of AgNPs. The biosynthesized AgNPs were subjected to rigorous characterization to elucidate their optical, morphological, structural, and elemental properties. In particular, UV-visible (UV-vis) spectroscopy is utilized (monitoring the surface plasmon resonance (SPR) peak) to optimize the synthesis parameters. This includes studying the effect of pH, temperature, and extract concentration for optimal growth, which is crucial for the formation and stability of AgNPs with the desired properties for effective photocatalytic performance[20]. The photocatalytic potential of biogenic AgNPs was assessed by degrading a dye or dye mixture under sunlight. In general, the degradation process was monitored spectroscopically, and understanding the mechanisms is crucial for enhancing its efficiency[12]. The impact of the treated wastewater is most commonly accessed on the germination of several plants like rice (*Oryza sativa*), mustard (*Brassica juncea*), and lentil (*Lens culinaris*). The lentil, rice, and mustard seeds are economically and important healthier crops for consumption and may be utilized to investigate the ecological and agricultural significance of the treated wastewater.

Herein, we report (i) the phytochemically biogenic synthesis of AgNPs using aqueous leaf extract of *Clerodendrum infortunatum (Linn.)*, (ii) characterize several properties (like optical, morphological, structural, and elemental investigation) of newly biosynthesized AgNPs, (iii) The effect of various parameters was systematically studied by UV-vis spectroscopy to obtain the optimal growth condition for the biogenic formation of AgNPs, (iv) the impact of biogenic AgNPs on the photocatalytic decomposition of crystal violet (CV), thioflavin T (TT), and methylene blue (MB) and their ternary mixture (chosen as a model dye contaminant and it signifies common dye) under the sunlight, with mechanisms of photocatalytic decomposition and (v) to investigate the environmental applicability of treated wastewater, seedling growths of rice (*Oryza sativa*), mustard (*Brassica juncea*), and lentil (*Lens culinaris*) plants were evaluated in the presence of treated wastewater. Preliminary findings support using treated wastewater to grow plants that preserve the ecological balance of essential water.

Result and discussion

UV-visible spectral analysis

The AgNPs could be effectively biosynthesized by employing phytochemicals from leaf extract (in aqueous medium) of *Clerodendrum infortunatum* as both reducing and capping agents. The initial indication for the biogenic synthesis of AgNPs was detected by the visual inspection of the color transformation for the solutions from light yellow to reddish yellow (Inset Fig. 1). Further, the biogenic synthesis of AgNPs was proven by UV–visible (UV-vis) spectrophotometer, which detected the characteristic absorbance band at λmax. It is widely known that AgNPs exhibit absorbance peaks at λmax. In this study, AgNPs show distinct surface plasmon resonance (SPR) bands (optical density) at ~ 420 nm (Fig. 1). The UV-vis absorbance is an optical characterization technique primarily used to detect the interaction between molecules in real-time[21]. The phenomenon involved in the collective oscillation of free electrons from the conduction band (CB) of metal excited by the incident light (photon) is called SPR (at λ_{max}), and intensity can be adjusted by regulating the composition, size, shape, structure, and medium of NPs[22].

Process optimization for biogenic synthesis of AgNPs

The optimization technique is crucial for controlling the morphology, stability, and production yield during the biogenic synthesis of NPs. UV-vis spectroscopy was utilized to determine the impact of each parameter on the formation of AgNPs shown in Figs. 2 and 3, and appropriate conditions were suggested to achieve the highest intensity at λmax[23]. The overall biogenic synthesis conditions could be optimized considering the results (at λ_{max}) of SPR peak (Fig. S1) intensity[24,25]. Figures 2 and 3 shows the several ranges of color changes that were seen during the production of the AgNPs under different factors. By adjusting several factors (such as reaction duration, temperature, pH, and plant extract concentration) of biogenic synthesis process for AgNPs was optimized. Suitable conditions were proposed to obtain the highest intensity of biogenic AgNPs at λ_{max} (find the details in Supplementary Information). So, the optimum conditions (physico-chemical) for the biogenic synthesis of the AgNPs were recommended for concentration of *Cledrdendrum infortunatum* leaf extract (2%), concentration of salt (4 mM, $AgNO_3$), pH condition (10.0), reaction time (60 min) and temperature (80 °C).

Size distribution and zeta potential

The Dynamic light scattering (DLS) is a sophisticated analytical technique applied to identify the size distribution profile and the average size (Z_{avg}.) of particles of the NPs. The neutral NPs are those whose zeta potentials vary from −10 and +10 mV. In general, stable NPs are those whose zeta potentials greater than −30 mV or +30 mV[26,27]. The zeta potential value of this biogenic synthesis of AgNPs is −20 (Fig. S2a), which indicates that

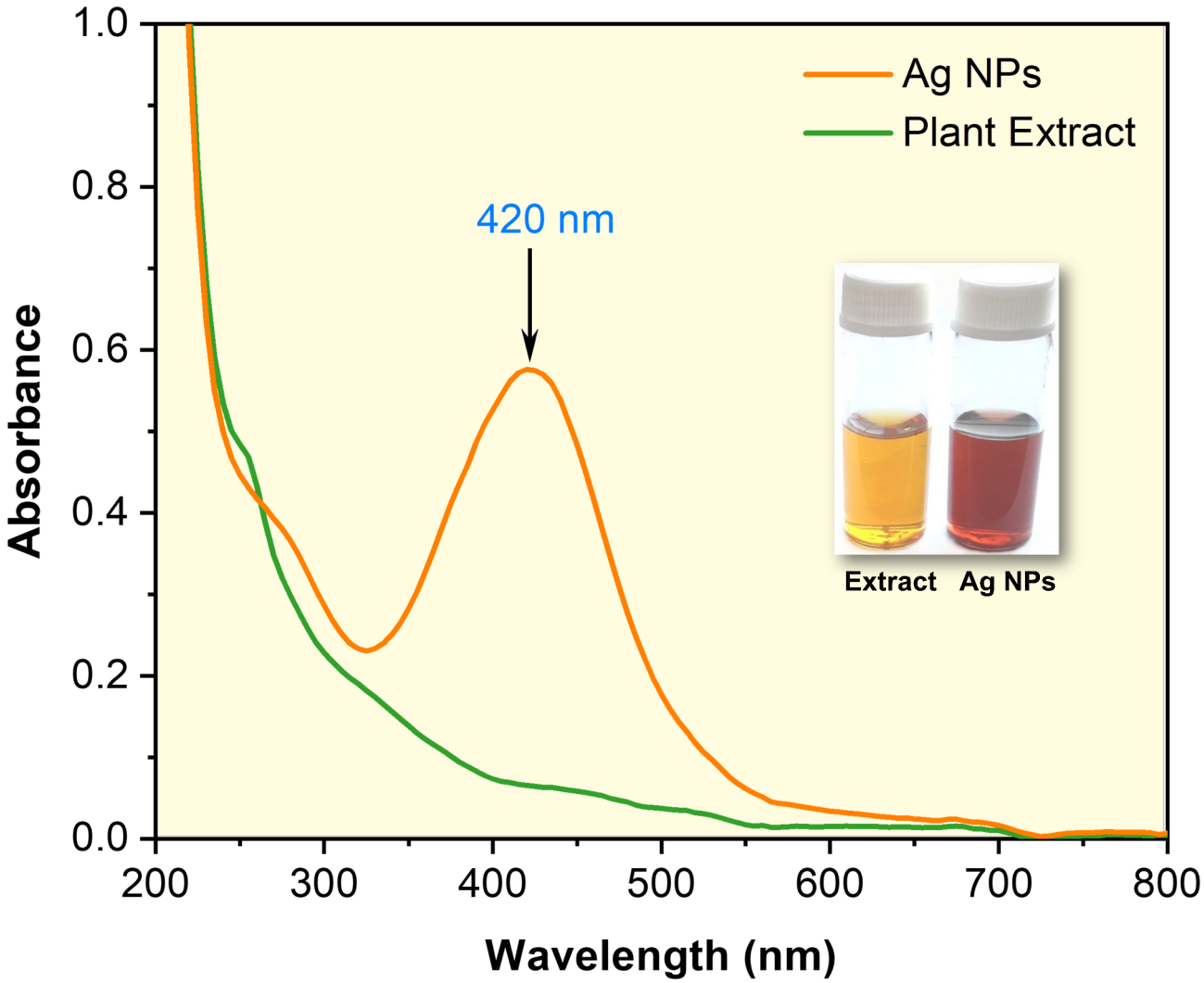

Fig. 1. (**a**) UV–vis absorbance spectra of the plant extract and biogenic synthesis of AgNPs. AgNPs show a distinct absorbance peak (λ_{max}) at 420 nm (Inset shows the visual color changes of the AgNPs solution after biosynthesis using plant extract solution).

the biogenic synthesized NPs are quite stable over a prolonged period. In addition, the average nano size of the biogenic synthesized AgNPs was 42.08 nm. The DLS technique directly determined the size distribution profile of stable AgNPs in the solution (Fig. S2b,c). For the biogenic AgNPs with a particle size distribution (percentile) characterized by $d_{10} = 12$ nm $d_{50} = 15.5$ nm, and $d_{95} = 25.5$ nm, where these values provide a detailed picture of the size distribution and uniformity (Fig. S2d). This means that 10% of the AgNPs have a diameter smaller than 12 nm. As the median (50%) particle size, this value suggests that the size of typical sample or most common AgNP is 15.5 nm. The 95% of particles smaller than 25.5 nm, this value shows that a small fraction of the particles is relatively larger, extending the upper end of the distribution. The distribution suggests a predominantly monodisperse sample, with a small percentage of larger particles is suitable for applications that benefit from size uniformity, such as catalysis activity, where both the specific surface area and reactivity can be influenced by particle size. The calculated polydispersity index for AgNPs was 0.579 indicating that these NPs were polydisperse. The coating layer of the biomolecules in the plant extracts may contain hydroxyl (–OH) and carboxylic (–COOH) groups (later discussed in the functional group section), which may be the cause of the significant negative charge value on the surface of the AgNPs. As a result, a strong negative charge value generates the electrostatic repulsion between the individual AgNPs, which may stop the NPs from aggregating[28]. The stability of the biogenic synthesized AgNPs was investigated using UV–vis spectrum analysis. Even after 20 days, there were no appreciable changes in the UV-vis spectra (at λ_{max}) position or intensity, indicating the stable size and size distribution (results not shown). As per the previous study, the key differences between chemically and phytochemically synthesized NPs regarding stability, biocompatibility, and efficacy are summarized in Table S4. This table provides a clear, comparative view to aid in choosing the right synthesis approach based on desired NP properties for specific applications.

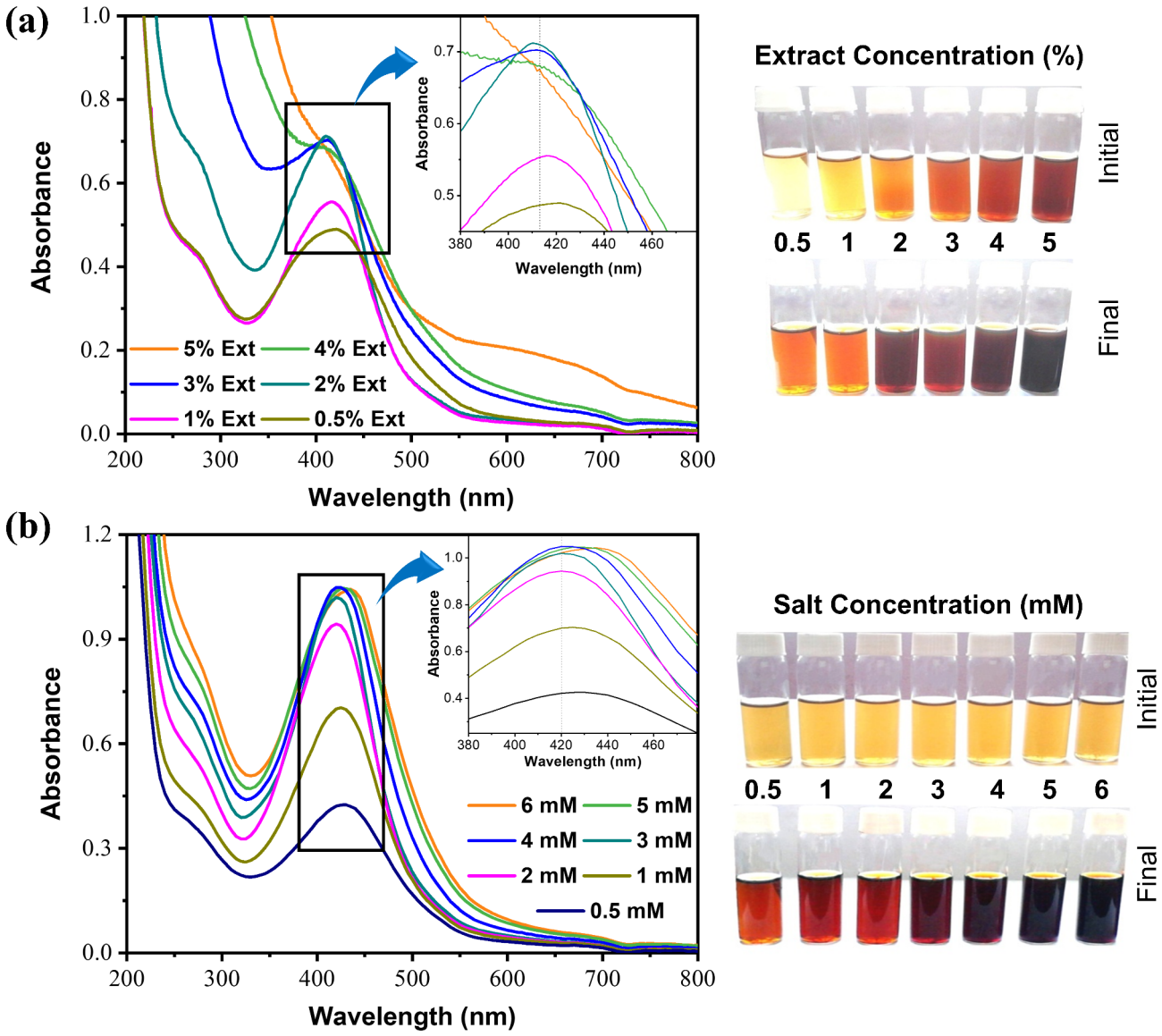

Fig. 2. (**a**) Plant extract-dependent UV–vis absorbance, (**b**) Precursor salt-dependent UV–vis absorbance of the biogenic AgNPs, and corresponding visual color change of the biogenic synthesis of AgNP.

Morphological studies and elemental analysis

The absorbance data provide strong shreds of evidence of the formation of biogenic synthesized AgNPs. The morphological and elemental analysis of the resultant NPs were further confirmed by the TEM (transmission electron microscopy) and EDX (energy dispersive X-ray spectroscopy) study. Moreover, the biogenic synthesized AgNPs had a homogeneous size distribution and were spherical. Notably, synthesized AgNPs are well separated, indicating that aggregation has not occurred. The TEM image in Fig. 4a shows that the size of AgNPs is less than 20 nm. The size of AgNPs determined by DLS is bigger than that determined by TEM due to the difference in the preparation process of the sample. So, the average hydrodynamic diameter of the AgNPs in solution is calculated by DLS but this covers not just the NPs core but also surrounded by solvent molecules and any biomolecules that have been adsorbed (such as polysaccharides, proteins, or other biomolecules of plant extract that coat the surface of the NPs)[29,30]. The hydration layer and the phytochemical coating may be partially or completely eliminated when NPs are dried on a grid during the sample preparation process for TEM. Hence, TEM is limited to measuring the solid metallic core alone, without any chemical or biological coverings. So, TEM images provide detailed information on the morphology and size of the AgNPs by allowing direct visualization of them[31,32]. The elemental composition of the formation of biogenic synthesized AgNPs can be determined with the help of EDX. The EDX spectrum of the biogenic synthesized AgNPs showed the existence of Ag element signals (Fig. 4b). While background signals for the impurities of Cu, C, and Si have also been identified, these could be caused by the carbon coating on the copper grid or by the copper grid itself. On the other hand, the remaining elements could be the result of carbon-containing biomolecules from the plant extract that have bound to AgNPs[33].

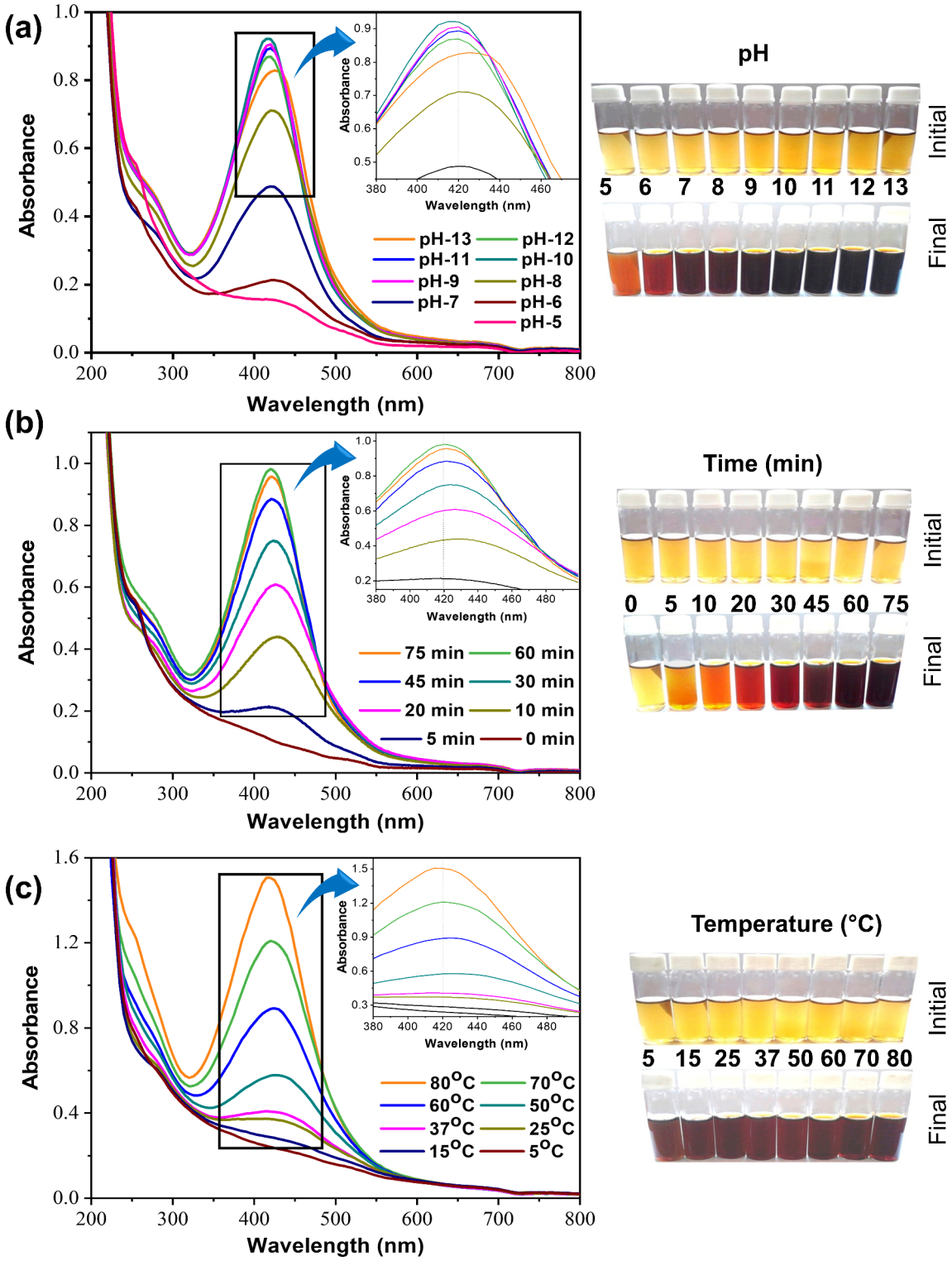

Fig. 3. (**a**) pH-dependent UV–vis absorbance, (**b**) Time-dependent UV–vis absorbance, (**c**) Temperature-dependent UV–vis absorbance of the biogenic synthesis of AgNPs, and corresponding visual color change of the biogenic synthesis of AgNPs.

Identification of phytochemicals and functional groups

Functional group analysis by FTIR

The Fourier Transform Electron Spectroscopy (FTIR) study was done to recognize the probable functional groups of biomolecules within the plant matrix that may be responsible for the biogenic synthesis of AgNPs (Fig. S3). As shown in Table S1, the FTIR spectrum of plant extract exhibited major characteristic peaks at 3393 cm^{-1}

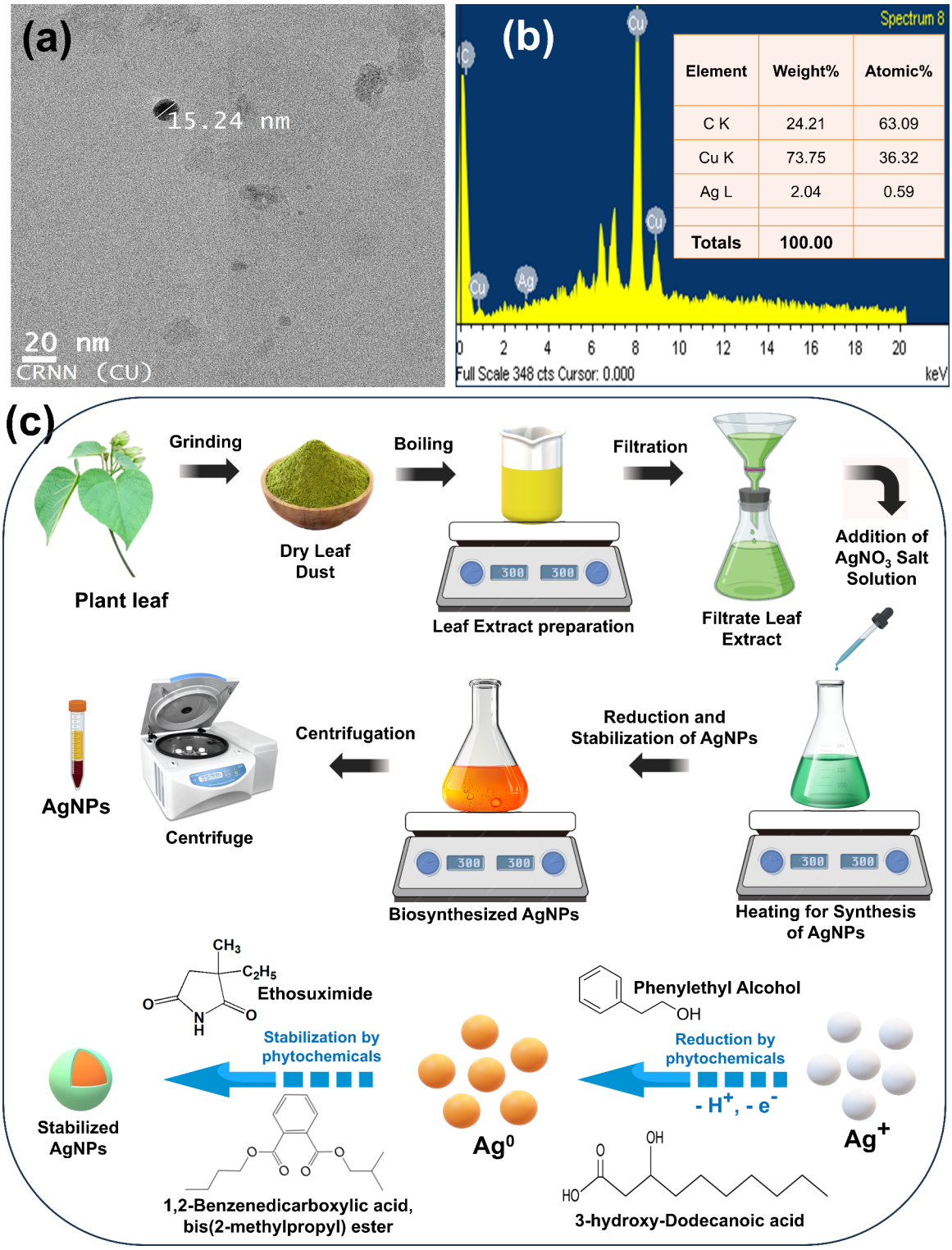

Fig. 4. The (**a**) TEM images and (**b**) EDX spectra (the inset shows the elemental analysis of the corresponding AgNPs) of the biogenic synthesis of AgNPs, and (**c**) Schematic representation of the biosynthesis of AgNPs using plant extract.

(for O–H stretching), 2925 cm^{-1}, 1407 cm^{-1} (for C–H stretching), 1603 cm^{-1} (for N–H and NH_2 bending), 1108 cm^{-1} (for C=O stretching), 763 cm^{-1} (for C–H bending) and 615 cm^{-1} (for C–Br stretching)[34–36]. These distinct peaks confirm that the extract contains several bioactive compounds (functional groups) that may function as a reductant for reducing the silver nitrate, hence facilitating the synthesis of AgNPs. On the other hand, FTIR spectra of biogenic AgNPs showed a shift in some characteristic peaks and the appearance of several

new peaks due to the interaction of bioactive compounds with AgNPs. It was noticed that peaks at 3393, 2925, 1603, 1407, 1108, 763, and 615 cm^{-1} in leaf extract were shifted towards 3403, 2919, 1619, 1384, 1158, 771, and 647 cm^{-1}, respectively. In addition, there was the emergence of new peaks at 1055 (for C=O stretching vibration of ester, carboxylic acids, and alcohol), 897 (for N–H waging modes of Amines), and 824 cm^{-1} (for C=C and C–H stretching vibration of hydrocarbon part of biomolecules) in AgNPs it may be due to interaction of biocompounds with AgNPs[35,37,38]. These findings supported that many biomolecules, especially O–H, COOH, COOR, R–O–R′, and amide (N–H, C=O) could be present in leaf extract, and these functional groups might be associated with reduction, binding, and stabilization of biogenic AgNPs.

Phytochemical screening by GC-MS

GC-MS analysis identified 45 major compounds in *Clerodendrum infortunatum* leaf extract (Table S2) which have a range of biological activities that might be responsible for the biogenic AgNPs. The peak mass spectrum of these major compounds was matched with the NIST mass spectral library[14,39]. However, analytical standards were not employed through the GC-MS analysis for definitive recognition of phytochemicals. Hence the presented results may be considered reasonable given the possibility for proper identification of phytochemicals. Already, the *Clerodendrum infortunatum* plant is reported to contain 9-Hexadecenoic acid (retention time, RT: 13.52 min), Hexadecane (RT: 16.05 min), tert-Hexadecanethiol (RT: 17.47 min), 1-Hexadecanol, 2-methyl- (RT: 27.63 min) and 2,5-Octadecadiynoic acid, methyl ester (RT: 30.63 min)[40–42]. For example, several alcohols were found in the extract with higher probability like 1-Hexadecanol, 2-methyl-, and Verrucarol. As well, many of the carboxylic compounds were identified in the extract: 1,7-Octadiene, 2,5-bis-(cis)-(2,2-dimethyl-3-carboxycyclopropyl)-9-Hexadecenoic acid; Dodecanoic acid, 3-hydroxy-; cis-10-Nonadecenoic acid. Briefly, there are also many ether compounds contained in samples: 2-Methyl-cis-7,8-epoxynonadecane, Ethanol, 2-(octadecyloxy)-. The extract contained considerable levels of certain esters, such as 2,5-Octadecadiynoic acid, methyl ester, Retinoic acid, and methyl ester. Several aldehydes were also found in the extract including. GC-MS chromatogram of the samples is provided in Supplementary Fig. S4. Hence it may be possible that FTIR-identified functional groups of the above phytochemicals may be responsible for the capping and reduction of biogenic AgNPs[43].

Probable mechanism for the biosynthesis of AgNPs

The mechanism behind the reduction and stabilization of AgNPs by phytochemicals is not adequately explained in the literature[44,45]. Reduction of ions, nucleation, and growth stages are the three primary steps in nanoparticles formation. Each stage relies on the characteristics of extract concentration, $AgNO_3$ concentration, time, temperature, and pH. The precursor salts $AgNO_3$ dissociate into silver (Ag^+) ions and nitrate (NO_3^-) ions in distilled water. Some researchers suggested that the reduction of silver ions to Ag^0 may be caused by the –OH groups found in phytochemicals (like phenolic acids, terpenoids, alcohols, polyphenols, and flavonoids)[46]. It's possible that reactive hydrogen atoms released during the tautomeric conversion of phytochemicals from enol to keto form could convert Ag^+ ions to Ag^0[47]. For example, Phenylethyl Alcohol, 3-hydroxy-Dodecanoic acid, 2-methyl-1-Hexadecanol, Verrucarol, etc. were found in the extract with higher probability identified by GC-MS and FTIR data. So, these biomolecules may be involved in the reduction of Ag^+ ion to Ag^0. The probable mechanism for producing AgNPs (using *Clerodendrum infortunatum* leaf extract) through the conversion of Ag^0 to AgNPs by phytochemicals is depicted in Fig. 4c. The plant extract contained considerable levels of alkaloids, proteins, saponin, etc., which may involved for the stabilization of AgNPs[17,48]. There are many compounds present in samples (extract and surface of AgNPs) like cis-10-Nonadecenoic acid, 9-hexadecenoic acid, 1,2-Benzenedicarboxylic acid, bis(2-methylpropyl) ester, Ethosuximide that may act as a stabilizer of AgNPs. This capping layer stabilizes the nanoparticles by electrostatic or steric repulsion and depending on the nature of the bio-compounds present in plant. The process is generally green, eco-friendly, and scalable, leveraging natural plant resources to produce stable AgNPs for various applications.

Photocatalytic degradation efficiency of AgNPs

The photocatalytic activity of the AgNPs on the degradation of crystal violet (CV), thioflavin T (TT), and methylene blue (MB) individually was estimated by determining the residual concentration of dyes by spectrophotometrically at peaks 412 nm, 590 nm, and 665 nm, respectively at distinct intervals of time (Fig. 5). In a ternary dye mixture solution (TT + CV + MB), there was not any noticeable shifting of the absorption peaks (Fig. 5d). Therefore, the determination of specific dyes may be possible in a mixture of ternary dyes. Three distinct peaks (413 nm, 593 nm, and 665 nm) corresponding to the dyes TT, CV, and MB occur in the absorption spectra concerning the photocatalytic degradation of the ternary mixture dyes (TT + CV + MB). There was no significant shifting of absorption peaks in the ternary mixture of dyes (TT + CV + MB) solution (Fig. S5d) and clearly distinguish between the three peaks in the ternary mixture of dyes compared to distinct peaks of individual dyes. So, the photodegradation efficiency of each dye was examined based on the absorbance maxima (λmax) values of each dye in the mixture (TT + CV + MB) for the current investigation[6,49]. Nowadays, the photocatalytic degradation of several dyes under sunlight using NPs is commonly studied to estimate the photocatalytic activity of NPs. The optical density of dyes before and after 30 min under sunlight without adding AgNPs suggested that there was no alteration or a slight in the intensity of optical density (Fig. S5). Hence, no significant changes in the concentration of dyes and their ternary mixtures were obtained in the absence of AgNP catalysts that confirm the dyes are highly photostable under sunlight[14]. The degradation of dyes in an aqueous solution was determined at a particular time of interval under sunlight by AgNP as catalysts (Fig. 5) and determined in terms of degradation percent, reaction kinetics, T_{50} (half-life), and T_{80} (time needed for 80% degradation)[51,52].

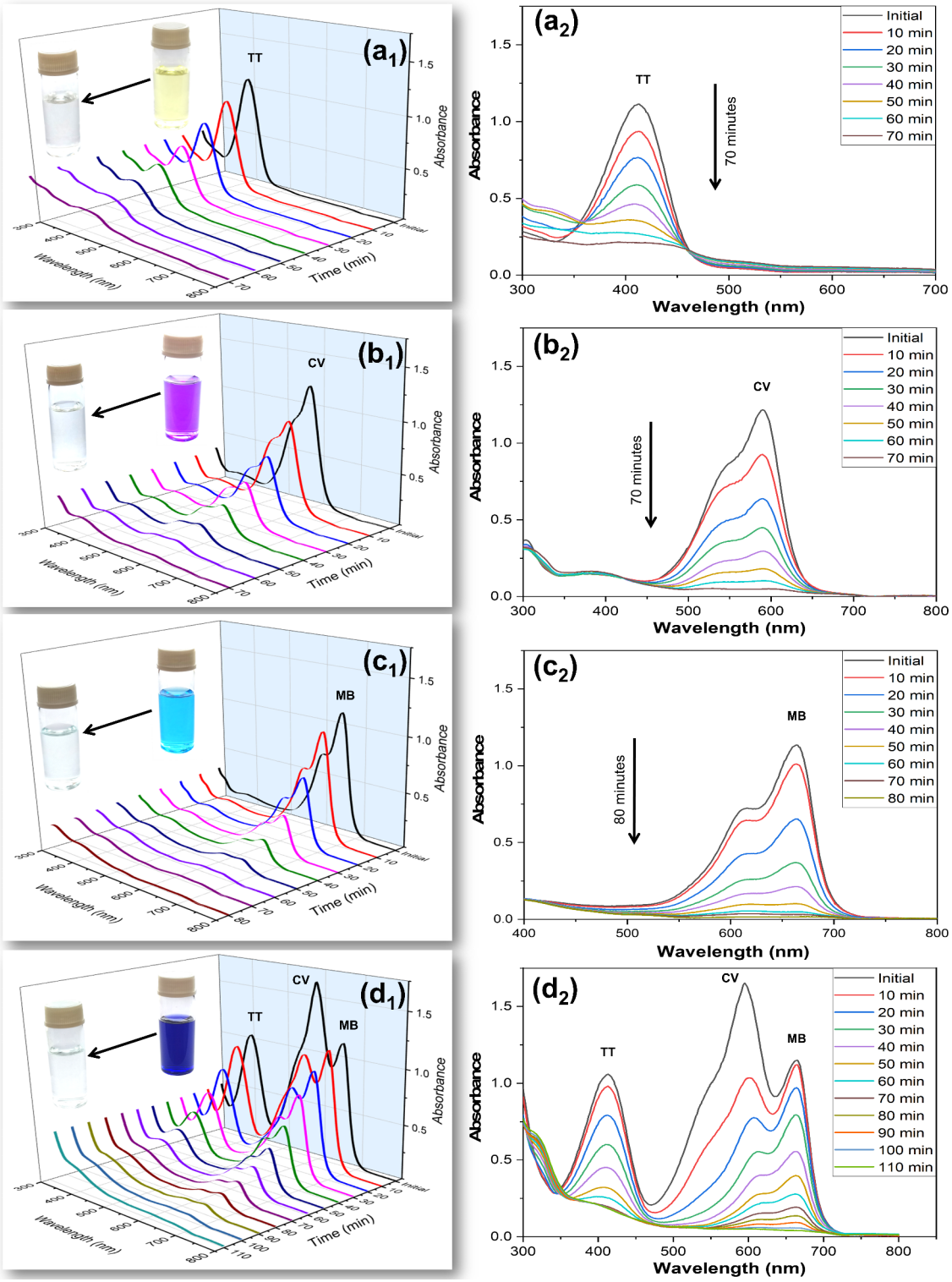

Fig. 5. Time-dependent 3D and 2D type degradation (UV–vis spectra) pattern for photocatalytic degradation of ($\mathbf{a_1}$, $\mathbf{a_2}$) TT, ($\mathbf{b_1}$, $\mathbf{b_2}$) CV ($\mathbf{c_1}$, $\mathbf{c_2}$), MB and ($\mathbf{d_1}$, $\mathbf{d_2}$) mixed ternary (TT + CV + MB) dyes in the presence of sunlight using AgNPs as a catalyst. The Inset of 3D figure shows the initial and final color change of the corresponding dye catalyzed by AgNPs.

Degradation percentage

The UV-vis spectroscopy was used to analyze the degradation pattern (3D and 2D type representation) of the dye in individual aqueous solutions as illustrated in Fig. 5a_1–c_3 and a_2–c_2 and for the ternary mixture of dyes in Fig. 5d_1,d_2. The degradation percent (using Eq. 1) of the dyes is displayed in Table 1. MB and CV dye exhibited

Dye Sample		Parameters				
		Degradation %	Time for Degradation (min)	Reaction Kinetics, k (min^{-1})	T_{50} (min)	T_{80} (min)
TT	For Unitary	82.83 ± 0.99^{d}	70	0.0268 ± 0.0011^{d}	25.89 ± 1.0617^{d}	60.10 ± 2.4651^{d}
	For ternary solution	82.89 ± 0.75^{d}	80	0.0247 ± 0.0008^{d}	28.11 ± 0.9290^{e}	65.28 ± 2.1570^{e}
CV	For Unitary	95.14 ± 0.73^{c}	70	0.0461 ± 0.0020^{b}	15.04 ± 0.6673^{b}	34.92 ± 1.5492^{b}
	For ternary solution	96.96 ± 0.28^{b}	100	0.0331 ± 0.0014^{c}	20.96 ± 0.8988^{c}	48.67 ± 2.0869^{c}
MB	For Unitary	98.50 ± 0.23^{a}	80	0.0593 ± 0.0014^{a}	11.70 ± 0.2762^{a}	27.16 ± 0.6412^{a}
	For ternary solution	95.39 ± 0.92^{c}	110	0.0316 ± 0.0023^{c}	21.98 ± 1.5479^{c}	51.04 ± 3.5938^{c}

Table 1. Comparing the performance of biogenic AgNP catalysts in the unitary and ternary mixture for the degradation of several dyes. Variations with different letters indicate statistical significance ($p < 0.05$) as per Duncan's multiple comparison studies. [T_{50} = Half-life and T_{80} = Time required for 80% degradation].

the fastest photodegradation in individual solutions, where ~ 98% of MB degraded within 80 min and ~ 95% of CV degraded within 70 min in the presence of sunlight using AgNPs (Table 1). However, TT dye showed moderate photodegradation in individual solutions, and ~ 83% of TT degraded within 70 min in the presence of sunlight using AgNPs (Table 1). A similar pattern for CV and MB was also observed in ternary mix dye solutions, where the photocatalytic degradation percentage of MB was ~ 95% within 110 min, and for CV it was ~ 97% within 100 min, while TT showed lower degradation i.e. ~ 83% of TT degraded within 80 min (Fig. S6). An earlier study shows that CuS is an effective photocatalyst for degrading individual dyes like CV (85%), RhB (81%), and MB (100%), and the degradation percentage was 89.8% (for CV), 88.7 (for RhB) and 92.1% (for MB) to their ternary mixture dye solution in 120 min[52]. This rapid degradation suggests that the molecular structure of MB and CV interact efficiently with the AgNPs, likely enabling efficient electron transfer that accelerates the breakdown process. The slower degradation of TT suggested that chemical structure may pose more resistance to the photocatalytic process, possibly due to strong molecular bonds, low adsorption affinity, electron transfer limitations, and potential aggregation behavior all contributing to resistance to degradation[53,54].

Degradation kinetics

The photocatalytic capabilities of the AgNPs were additionally estimated using reaction kinetics of the photodegradation of dyes (using Eq. 2) as illustrated in Fig. S7a–c. The research data can be fitted in a straight line for the dye degradation with a good linear ($R^2 > 0.990$) regression coefficient confirms a strong fit to pseudo-first-order kinetics, indicating consistent and predictable degradation behavior (shown in Figs. S7a–c)[55,56]. Table 1 displays the reaction kinetic rate constants (k) for the dye degradation. The highest kinetics rate of photodegradation observed for MB was 0.0593 min^{-1}, and CV shows a moderate kinetics rate of 0.0461 min^{-1}, while TT shows a lower kinetics rate of 0.0268 min^{-1} in the case of individual dye (Table 1). Similar manner to the individual dyes, the rate constants of dye in the ternary mixture were found to be 0.0331 min^{-1} for the CV, and for the case of MB, it was 0.0316 min^{-1}. The kinetics rate constants for TT in the ternary mixture were calculated to be 0.0247 min^{-1} in the ternary mixture based on their catalytic action detected at their corresponding λmax values. According to a previous study, the reaction kinetics of TG-cl-PAA/Fe_3O_4 (magnetic tragacanth gum-crosslinked-poly(acrylic acid) nanocomposite hydrogel) for TT dye in individual solution (0.0187 min^{-1}) and in ternary mix solution (0.0193 min^{-1}) shows an excellent photocatalytic activity[6]. This result supports the previous observation of TT for moderate degradation percentage, likely due to its more resistant chemical structure or lower adsorption affinity to AgNPs, as discussed. CV showed a moderate rate constant, which is slightly lower than MB but still indicates a relatively fast degradation process. The moderate rate constant for CV suggests that it also interacts well with AgNPs, though slightly less efficient than MB. The decrease in rate constants of dyes in the ternary dye mixture is attributed to the competition among dye molecules for the active sites on the AgNPs surface. When multiple dyes are present, they may compete for adsorption onto optically active centers on the AgNPs, leading to a lower availability of reactive sites per dye molecule. This competitive effect is typical in mixed dye solutions and illustrates the challenges of achieving efficient degradation in complex, and multi-component wastewater environment[57,58].

Half-life with needed time for 80% dye degradation

The T_{50} (half-life) and T_{80} (needed time for 80% degradation) of a kinetics reaction (dye degradation) are often calculated using the Eqs. (3) and (4), respectively, and results are shown in Table 1. This type of parameter is frequently utilized for reaction kinetics to describe how quickly a substance degrades during a photocatalytic process. The calculated half-life for MB, CV, and TT were found to be 11.17 min, 15.04 min, and 25.89 min, respectively in an individual solution in the presence of sunlight using the AgNPs (Table 1). However, the calculated half-life for degradation of CV (20.96 min) was comparable to MB (21.95 min) in ternary mixture solution while the calculated half-life value for degradation of TT (28.11 min) was slightly high compared to the degradation of CV and TT in ternary mixture solution (Table 1). Similarly, the calculated T_{80} values of MB, CV, and TT dyes were found to be 27.16 min, 34.92 min, and 60.10 min in individual solutions (Table 1), whereas 51.04 min, 48.67 min, and 65.28 min in the ternary mixture (Table 1), respectively catalyze by AgNPs. Earlier research shows that the half-life and T_{80} values of Fe-CdO NPs for degradation of MB dyes were 43.04 and 99.93 min, respectively, and in binary mixtures, they were 51.33 and 119.18 min[50]. Table S3 presents a comparison examination of dye degradation under the current research with those previously published. The

comparison data showed that, in contrast to the previously published data, the degradation time in our work was faster in every instance, and the catalytic reaction rate was either unchanged or increased in the current investigation[59]. The results of half-life and T_{80} provide valuable insights into the efficiency and quantify the speed of photodegradation, comparing it across different dyes and solution conditions. Interestingly, the T_{50} and T_{80} values for MB and CV in mixtures are lower than the TT dye values, indicating that in competitive environments, MB and CV may degrade more quickly due to the initial rapid reaction rate, though degradation of TT dye remains slower. This pattern may arise from the tendency of AgNPs to initially target the more reactive dyes (MB and CV) in a mixture, leaving TT as a secondary target in the later stages of degradation. The comparative data suggest that AgNPs exhibit consistently faster degradation times in each case, validating their enhanced catalytic capabilities for dye degradation. The distinct variations in T_{50} and T_{80} values for different dyes can be attributed to their unique chemical structures and the specific interactions they have with the ROS generated during the photocatalytic process. Faster T_{50} and T_{80} values across both conditions point to their potential as more effective photocatalysts in environmental applications, especially in treating dye-laden wastewater.

Reusable efficiency of AgNP catalysts

The recycling of the majority of catalysts was not easy or actual practical application methods because of several limitations, such as time-consuming separation, washing, and drying processes, among others. Therefore, it was determined if the AgNP catalysts could be reused for a practical application in the removal of colors from aqueous solutions. After each cycle of dye degradation reaction, the AgNPs catalysts were recovered by centrifugation and washed with MiliQ water and ethanol then reused for the next round of the same experiment[60]. Figure 6a shows the reusability of the AgNPs for the degradation of a mixture of dyes (TT + CV + MB) in an aqueous solution in the catalytic reaction cycle. The AgNP catalyst exhibited no noticeable decline in photocatalytic activity (< 9–12% for each dye) over its four cycles of degradation of ternary mixed dye solution so, further it may be used for many cycles. Their tiny mass losses in every cycling phase during handling into the dye reaction medium may be the cause of the negligible drop in photocatalytic efficiency[58,61,62]. This could be a result of some dye molecules that have degraded and adhered to the surface of AgNPs[12]. The study confirms that biogenic AgNPs are highly effective in degrading both individual and mixed dye solutions, following pseudo-first-order kinetics. The insights gained from the kinetic analysis can inform further optimization and practical application of AgNP-based photocatalytic systems for wastewater treatment. These findings reinforce the potential of biogenic AgNPs in environmental remediation efforts, offering a sustainable and efficient solution for the degradation of harmful dye pollutants.

Mechanism of photocatalysis for dye degradation

A probable mechanism of the photocatalytic degradation process for the studied dyes using the sunlight and AgNP photocatalysts system is shown in Fig. 6b. Surface plasmon resonance (SPR) is a phenomenon seen in AgNPs, whereby free electrons on the surface resonate of AgNPs with the electromagnetic field of light, particularly at particular wavelengths (often in the UV-vis range)[63]. In the photocatalysis process, the photons (beams of sunlight) are absorbed by a photocatalyst (AgNP) causing photoexcitation to create electron-hole pairs. These pairs subsequently engage in redox reactions with adsorbed species on the catalyst surface, ultimately resulting in the degradation of dyes in water[64,65]. The band gap energy of AgNPs was found to be ~ 3.30 eV according to Tauc ($(\alpha h\upsilon)^2$ vs. $h\upsilon$) plot as shown in Fig. S8.

The process of photocatalysis for dye degradation involves three stages[58–60]:

Photoexcitation The semiconductor is composed of two distinct energy bands including the valence band (VB) or ground state and the conduction band (CB) or higher energy state and their difference is known as the energy gap (Eg). When a semiconductor (AgNP) is struck by a beam of sunlight (photon) causes photoexcitation (electron excitation), the photoelectron is shifted from the VB to the CB due to the absorption of radiation. As a result of this photoexcitation, a hole (h+) and reactive electrons (e•–) are generated on the VB and CB, respectively[69,70].

Redox reactions The extremely reactive holes (h^+) in the VB and reactive electrons ($e•^-$) in the CB can engage in redox reactions with adsorbed species on the surface of AgNP catalyst. The main ROS such as hydroxyl radicals ($OH^•$) and superoxide radicals ($O_2^{•-}$) is generated from the oxidation of water (or hydroxide ions) by the holes (h^+) and from the reduction of oxygen molecules by the excited electrons ($e•^-$), respectively[69]. Extremely reactive radicals including hydroxyl radicals and superoxide radicals are produced when the photogenerated substances (h^+/e^-) interact with the water of the medium[66,71].

Degradation of dyes The ROS (especially $OH^•$) generated on the surface of AgNPs interacts with the dyes (MB, CV, and TT) molecules, causing oxidative degradation of dyes. Both MB and CV dye are aromatic compounds with conjugated systems and are highly susceptible to attack by hydroxyl and superoxide radicals. These radicals target the chromophoric groups of dyes, primarily the aromatic rings and the nitrogen-containing structures responsible for color. This reaction ultimately breaks down the dye molecules into smaller, and colorless fragments[72]. The TT degradation proceeds similarly but at a slower rate and the chemical structure includes more complex ring systems and possibly stronger intramolecular interactions making it slightly more resistant to ROS attack. TT may require more energy or additional exposure to sunlight to break its bonds effectively. The ROS-mediated degradation typically proceeds through several steps, where large dye molecules are broken into intermediate compounds (e.g., smaller aromatic fragments, amines, and eventually simple acids)[73,74]. Finally, the smaller intermediate fragments are further oxidized by continuous ROS attacks and may be degraded possibly to nontoxic products such as mineral acids, H_2O, and CO_2[76,77]. In summary, the primary way that AgNPs

demonstrate photocatalytic activity is by producing ROS in response to light irradiation. This process allows the AgNPs to break down contaminants. So, AgNPs have distinct optical characteristics, particularly surface plasmon resonance, and these properties are primarily responsible for their exceptional photocatalytic performance[56,77]. Even though the same amount of dye was used in each experiment, the rate of degradation showed varying values for each dye at the same time. The targeted chemical structure of dye may have an impact on variations in degradation rates[78,79]. Since the surface of AgNPs is covered in phytochemicals that may carry the matrix for reaction and aid in boosting the catalysis reaction rate. So, AgNPs synthesized using plant extracts may have greater catalytic activity[15,37].

Eco-toxicological assessment of treated dye solution

The eco-toxicological impact of treated wastewater (treated dye solution) on seedling growth of three types of plants such as rice (*Oryza sativa*), mustard (*Brassica juncea*), and lentil (*Lens culinaris*) plants from the pre-germinated seeds were performed to evaluate the sustainability and suitability of the overall photocatalytic method concerning the probable reuse of the treated dye solution.

Effect on seedling growth

Pre-germinated (2 days) Rice, Mustard, and Lentil seeds were used for analysis of seedling growth in the aqueous solution of pollutant dyes and their ternary mixtures before and after the photocatalytic degradation (removal of dyes by AgNPs), and control (only sterile distilled water). The seedling growth was observed after the 7 days of germination periods as illustrated in Fig. 7. The results exhibited a significant (<0.05) inhibitory effect of the aqueous solution of dyes and their mixtures (before degradation) in the root length for the three types of plants like mustard (Fig. 7a), lentil (Fig. 7b) and rice (Fig. 7c) plants. Similarly, very strong inhibition was observed for dye solutions and their mixtures (before degradation) in the case of shoot length for the three types of plants such as mustard, lentil, and rice plants (Fig. 7). However, treated wastewater showed no inhibitory phytotoxic effect on shoot, and root elongation on mustard, lentil, and rice plants (Fig. 7). The observed seedling germination of treated wastewater (photodegraded by AgNPs) showed healthier growth, much-improved, and almost similar types of growth of plants as compared to the control (only sterile distilled water) plants. A similar effect of treated water on seed germination has also been described previously, where photodegraded treated water (MB, CV, and rhodamine B dye mixture treated by graphene nanosheets) showed similar growth to control water, indicating non-toxic behavior but dyes and their mixtures inhibited wheat plant growth[12,80]. In the earlier study, MB solution strongly inhibited root germination in wheat and gram plants, while treated wastewater (MB dye treated by Nano-Carbon) showed improved, and healthier growth, resulting in healthier root and shoot parts[81,82]. Preliminary findings suggest that treated wastewater may be utilized for cultivating plants that can sustain the ecological balance of the necessary water. This technique can further lessen for reducing the overuse of natural resources and further encourage the reuse of water resources to at least for the non-edible plants including lawns grass, and gardens. However, more detailed research needs to be done regarding edible plants. Therefore, additional in-depth research is obligatory to study the eco-toxicity of treated wastewater to several categories and their ecosystems.

Experimental section

Materials

The substances silver nitrate (99.0%, $AgNO_3$), methylene blue (MB), and thioflavin T (TT) were purchased from MERCK (India), and crystal violet (CV) was procured from LobaChem, Mumbai, India. The remaining chemicals employed in every experiment, were pure analytical grade and required no additional purification. Throughout the investigation, Milli-Q (Millipore Corp., Billerica, MA) water was utilized. All glassware was washed thoroughly, rinsed many times with water (Milli-Q), and finally, dried in the Hot Air oven at 60 °C.

Collection, identification, and preparation of leaf extract

The Fresh and healthy leaves of the plant *Clerodendrum infortunatum* L. were gathered from the Bidhan Chandra Krishi Viswavidyalaya (BCKV) campus (Latitude 22.9452° N, Longitude 88.5336° E, Altitude 17) in West Bengal (WB), India. Central National Herbarium (CAL), Howrah, Botanical Survey of India (BSI) undertook the identification of the plant material (Specimen No. SVU/SG/002) used in our study. A voucher specimen of this plant material has been deposited (Docket No: HBKC0310241) in the Department of Botany, Kalna College (Purba Bardhaman, WB, India) for future reference. Then leaves were cleaned numerous periods with water (distilled) and shed dry at room temperature. After the leaves are completely dried, they chopped into tiny pieces and processed into a fine powder using a machine grinder. Exactly the weight of 18 g fine powder of *C. infortunatum* leaves was placed in an Erlenmeyer flask (size: 500 mL) filled with 300 mL of water (Milli-Q) and then heated at 80 °C for 1 h. The solutions were then allowed to gradually cool to reach room temperature before being filtered through Whatman filter paper (No. 40). The resulting supernatant solution (6% w/v) was then kept for subsequent experimental investigation in the refrigerator at 4 °C. Afterward, the filtrate solution was applied as a stabilizing and also reducing agent for the biogenic production of AgNPs. In addition, the pH of the leaf extract solution was found to be 6.90.

Biogenic synthesis of AgNPs

In a typical synthesis of AgNPs, 2 mL aqueous leaves extract of *Clerodendrum infortunatum* was mixed with 8 mL of aqueous salt (1mM, silver nitrate) solution. Afterward, this reaction mixture was transferred in a dark condition (set pH at 7) for 1 h heated to 70 °C, and observed the color change. The preliminary sign for the biogenic synthesis of AgNPs was observed by the color transformation of the reaction medium from light

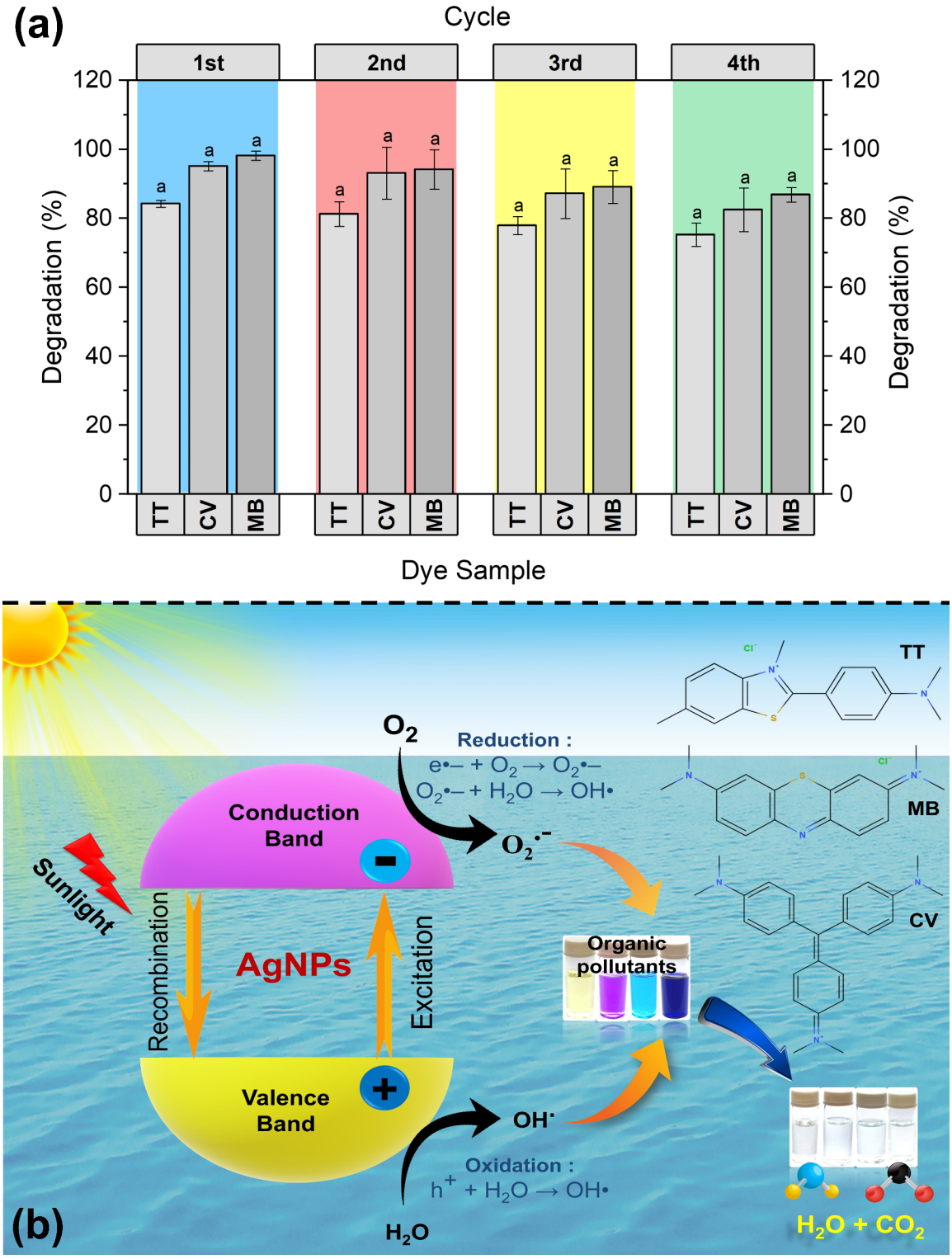

Fig. 6. (**a**) The recycling efficiency of AgNP catalysts for degradation of crystal violet (CV), thioflavin T (TT), and methylene blue (MB) in ternary mixed aqueous solution after four successive runs. Data were embodied as mean ± standard deviation and the same letter is not significantly ($p > 0.05$) dissimilar as per Duncan's multiple range tests. (**b**) Scheme showing the mechanism of photocatalytic degradation pathways for dyes in the presence of sunlight using biogenic AgNPs as a catalyst in water.

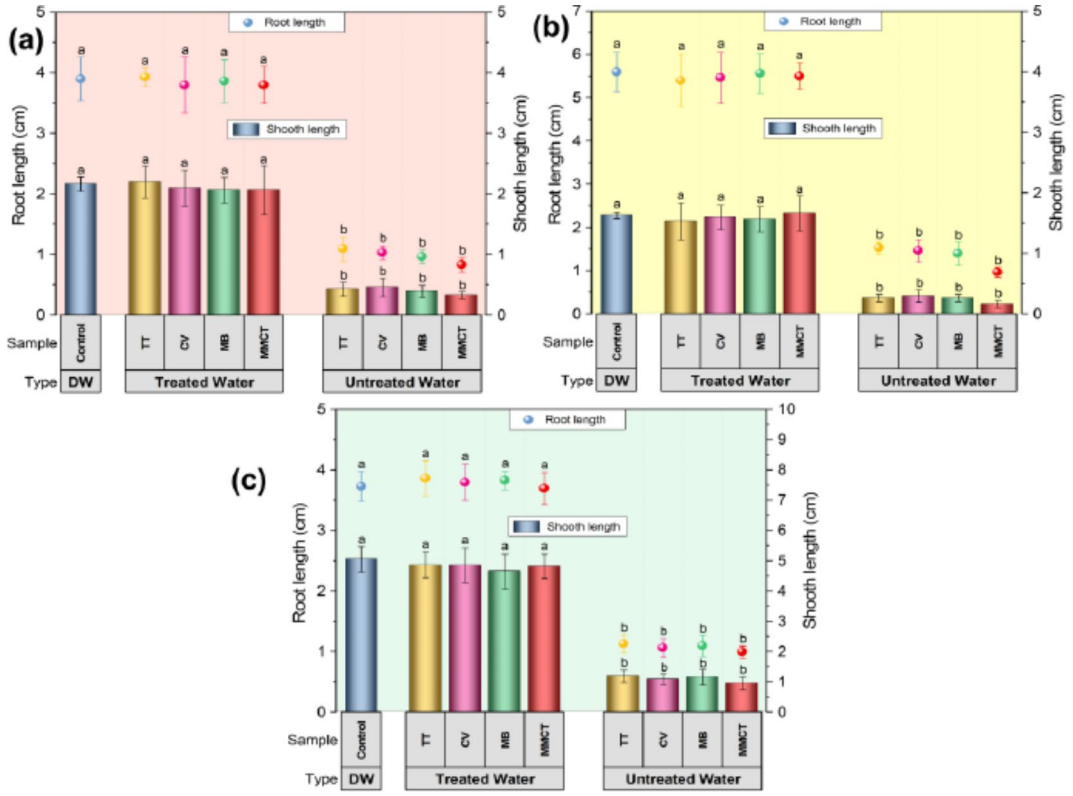

Fig. 7. The eco-toxicological impact of dyes and their ternary mixtures before and after the photocatalytic degradation (removal of dyes by AgNPs) and control (only sterile distilled water) on seedling growth of three types of plants (**a**) lentil (*Lens culinaris*), (**b**) mustard (*Brassica juncea*), and (**c**) rice (*Oryza sativa*) plants. Variations with different letters indicate statistical significance ($p < 0.05$) as per Duncan's multiple comparison studies [Bars indicate standard error (± SE); DW: Distilled Water].

yellow to golden yellow. However, the formation (growth kinetics) of AgNPs were confirmed by determining the absorbance of the reaction medium by UV-vis spectroscopy (scan range of 200–800 nm).

Optimization of biogenic synthesis conditions

To evaluate the influence of various parameters like the concentration of plant extract (0.5-5%), concentrations of the salt (0.5-6 mM), several pH values (5–13), various time (0–75 min), and reaction temperatures (5–80 °C) for the biogenic synthesis of AgNPs were assessed in dark conditions. The effect of these parameters on the biosynthesis of AgNPs was monitored by measuring the surface resonance plasmon (SPR) intensity of the solution using UV–vis spectroscopy. The biosynthesized AgNPs were reserved in an air-tight container at 4 °C temperature for further experiment.

Instrumentation for nano characterization

The UV-vis spectra of biogenic synthesized AgNPs were monitored by spectrophotometer (Varian, Model: Cary 50) at ambient temperature and scan range from 200 to 800 nm. Transmission Electron Microscopy (TEM; JEOL, Model: JEM-2100) in conjunction with an Energy Dispersive X-ray spectroscopy (EDX; Oxford Instruments, UK) detector and apparatus operating at an acceleration voltage of 200 kV were applied to analyze the size, shape, and elemental composition of the biogenic synthesized AgNPs. The sample was prepared onto a carbon-coated copper grid (size: 200 mesh) and placed in desiccators to allow complete evaporation of water at room temperature for TEM analysis. To identify the particle size, zeta-potentials, and polydispersity index of the biogenic synthesized AgNPs in the medium were measured by Dynamic Light Scattering (DLS, Malvern, UK, Model: Nano-ZS) using cuvettes (polystyrene type). The Fourier Transformation Infrared spectra (FTIR, Perkin Elmer L 120–000 A) of the experimental samples were recorded in the spectral region of 4000 to 450 cm^{-1} and applied at a 4.0 cm^{-1} resolution. The biogenic synthesized AgNPs and leaf extract were subjected to centrifugation at 15,000 rpm for 30 min before the FTIR analysis and dried for 3 h in a hot air oven (at 50 °C temp) and were ground with dehydrated potassium bromide (100:1). Details of the procedure for sample (leaf extract) preparation, instrumental conditions and identification of probable biomolecules for GC-MS analysis were discussed in Supplementary Information (see details in Supplementary methods).

Photocatalytic experiments

The photocatalytic efficiency of AgNPs was explored through the photocatalytic degradation of crystal violet (CV), thioflavin T (TT), and methylene blue (MB) in unitary, and ternary dye solutions in the presence of stable sunlight. The CV, MB, and TT, dye stock solutions were first made at a necessary concentration for further studies. In this study, 1 mL of each dye solution (1 ppm) was taken in 250 mL conical for the unitary batch system. Three dyes (1 ppm) were combined in volume ratios 1:1:1 (v/v/v) for the ternary batch system in a 250 mL conical. Subsequently, 10 mL of AgNPs (1 mg/mL) catalysts were added in conical for each unitary, and ternary batch studies, respectively. Finally, the total volume was filled up to a volume of 100 mL by the addition of water (Milli-Q) with natural pH at room (25 °C) temperature under sunlight. In this study, the experimental solution was taken in a centrifuged (approx. 15000 rpm) and the supernatant was collected in a 3 mL quartz cuvette and examined at regular intervals of time by the UV-vis spectrophotometer. So, the change in the absorbance (intensity at λmax) data of the dyes with time interval indicates the degradation process of dyes[77,83].

Dye sample analysis

The UV–vis spectroscopy (Varian, Cary 50) was used to investigate the residual part of the dye in unitary and ternary dye solutions in every batch system at room temperature in definite intervals of time.

The photocatalytic activity of AgNPs can be estimated using the following formula[50]:

$$\text{Dye Degradation}(\%) = \frac{(C_0 - C_t)}{C_0} \times 100 \tag{1}$$

where C_0 is the preliminary optical density of the dye medium and C_t is the optical density of the dye medium at definite intervals (t) of time. On the other hand, the apparent rate constant (k) is derived from the first-order kinetics law which is expressed as follows[51]:

$$ln\frac{C_t}{C_0} = -kt \tag{2}$$

The photocatalytic performance of the biogenic AgNPs for degradation of dyes in solutions was determined in terms of half-life (T_{50}) of dyes, and also the time needed for 80% degradation of the dyes (T_{80}) was calculated as follows[50,51]:

$$T_{50} = \frac{\ln 2}{k} = \frac{0.693}{k} \tag{3}$$

$$T_{80} = \frac{\ln 4}{k} = \frac{1.609}{k} \tag{4}$$

Eco-toxicological Bioassay

The ecological safety of the treated wastewater was assessed regarding the phytotoxic impact on morphological or seedling (shoot and root length) properties of lentil (*Lens culinaris)*, rice (*Oryza sativa)*, and mustard *(Brassica juncea)* seeds during the growth period. Seedling growth is recognized as a simple, fast generally applied acute phytotoxicity technique with several benefits including sensitivity, simplicity, and cost-effectiveness, and also suitable for unstable samples or chemicals. After centrifugation (at approx. 15000 rpm) of photocatalytic reaction solution, only the supernatant was collected and examined for further toxicity studies.

Growth conditions and Seedlings growth

The seeds were obtained from the Dept. of Agronomy, BCKV, WB, India. They were soaked in a 10% (v/v) sodium hypochlorite medium for ten minutes, then properly rinsed with water (distilled) to remove any remaining dust particles and allowed to dry at room temperature. Pre-germinated (for two days) and healthy seeds were employed in hydroponic growth systems to monitor the seedling growth under the treated wastewater (photocatalyzed by AgNPs) in comparison to polluted dyes and their mixture. Pre-germinated seeds (20 nos.) were placed in a petri dish with almost identical water-soaked filter paper (Whatman 42 Filter, 150 mm) that contained (5.0 mL each) (i) dyes and their ternary mix; (ii) their corresponding treated wastewater, and (iii) sterile distilled water to investigate the seedling growth of the plants. The Petri dishes were labeled following the treatment, covered, and enveloped with Parafilm tape and finally put in a plant-growth incubator at a particular temperature (28 ± 2 °C) at ~80% relative humidity with day-night cycles (12 h each). Water (sterile distilled) was added to the Petri dishes as needed to regulate the moisture content. After the seventh day, the length of the roots and shoots of the sample were measured for each Petri dishes[84].

Statistical analysis

In this work, all groups of tests were conducted in triplicate or more, and the data were provided as mean ± standard deviations (mean± SD). The Statistical Package for Social Sciences (SPSS and Version 16.0) was applied to determine the statistical studies. A one-way analysis of variance (ANOVA) was applied by the software (SPSS), and Duncan's multiple tests were applied to determine the significance ($p < 0.05$) of every mean value.

Conclusion

This study successfully demonstrates a green approach for synthesizing biogenic AgNPs using the aqueous leaf extract of *Clerodendrum infortunatum* (Linn.) providing a sustainable and efficient approach to water treatment.

AgNPs are spherical, with a size of ~20 nm, pure, and stable for a long time. Spectroscopic optimization enabled control over the synthesis parameters, resulting in AgNPs with enhanced photocatalytic properties. The biogenic AgNPs effectively decomposed ternary dye (TT + CV + MB) mixture under sunlight irradiation, showcasing their potential for removing complex dye contaminants from wastewater concerning degradation percentage (82.89–96.96% within 110 min), kinetics ($k = 0.0247–0.0331\ min^{-1}$), T_{50} (20.96–28.11 min), and T_{80} (48.67–65.28 min) and also easily recovered and reused upto many cycles. The probable mechanism of photocatalytic decomposition of dyes has also been discussed. Furthermore, the ecotoxicological assessment of treated wastewater highlights its environmental applicability. Growth tests with rice (*Oryza sativa*), mustard (*Brassica juncea*), and lentil (*Lens culinaris*) seedlings indicated that the treated water support healthy plant growth, suggesting its potential for agricultural use without disrupting ecological balance. Overall, the study underscores the feasibility of biogenic AgNPs as an eco-friendly alternative for efficient photocatalytic degradation of complex dye contaminants in wastewater which could be reused in real-life applications. The successful integration of ecological safety assessments further ensures that the treated wastewater can be safely used for agricultural purpose, promoting sustainable development and environmental conservation. Future work may expand on these findings and exploring the efficacy of AgNPs against other contaminants and further evaluating the long-term impacts of treated water on soil and crop health.

Data availability

The datasets used and/or analysed during the current study available from the corresponding author on reasonable request.

Received: 30 September 2024; Accepted: 4 December 2024
Published online: 28 December 2024

References

1. Dutta, S. et al. Contamination of textile dyes in aquatic environment: adverse impacts on aquatic ecosystem and human health, and its management using bioremediation. *J. Environ. Manag.* **353**, 120103 (2024).
2. Manzoor, M. H. et al. Wastewater treatment using metal-organic frameworks (MOFs). *Appl. Mater. Today*. **40**, 102358 (2024).
3. Mukherjee, A. et al. Dissipation behaviour and risk assessment of fipronil and its metabolites in paddy ecosystem using GC-ECD and confirmation by GC-MS/MS. *Heliyon* **7** (2021).
4. Oladoye, P. O., Ajiboye, T. O., Omotola, E. O. & Oyewola, O. J. Methylene blue dye: toxicity and potential elimination technology from wastewater. *Results Eng.* **16**, 100678 (2022).
5. Mani, S. & Bharagava, R. N. Exposure to crystal violet, its toxic, genotoxic and carcinogenic effects on environment and its degradation and detoxification for environmental safety. In *Reviews of Environmental Contamination and Toxicology*, vol. 237 (ed De Voogt, W. P.) 71–104 (Springer International Publishing, 2016).
6. Jaymand, M. Biosorptive removal of cationic dyes from ternary system using a magnetic nanocomposite hydrogel based on modified tragacanth gum. *Carbohydr. Polym. Technol. Appl.* **7**, 100403 (2024).
7. Solayman, H. M. et al. Performance evaluation of dye wastewater treatment technologies: a review. *J. Environ. Chem. Eng.* **11**, 109610 (2023).
8. Choudhary, S. et al. Phyco-synthesis of silver nanoparticles by environmentally safe approach and their applications. *Sci. Rep.* **14**, (2024).
9. Jafarzadeh, S. et al. Green synthesis of nanomaterials for smart biopolymer packaging: challenges and outlooks. *J. Nanostruct. Chem.* https://doi.org/10.1007/s40097-023-00527-3 (2023).
10. Roy, S. & Das, T. K. Effect of biosynthesized silver nanoparticles on the growth and some biochemical parameters of @@ aspergillus foetidus. *J. Environ. Chem. Eng.* **4**, 1574–1583 (2016).
11. Ma, H. Y., Zhao, L., Wang, D. B., Zhang, H. & Guo, L. H. Dynamic tracking of highly toxic intermediates in photocatalytic degradation of pentachlorophenol by continuous flow chemiluminescence. *Environ. Sci. Technol.* **52**, 2870–2877 (2018).
12. Gunture et al. Soluble graphene nanosheets for the sunlight-induced photodegradation of the mixture of dyes and its environmental assessment. *Sci. Rep.* **9**, 2522 (2019).
13. Arshad, F. et al. Bioinspired and green synthesis of silver nanoparticles for medical applications: a green perspective. *Appl. Biochem. Biotechnol.* **196**, 3636–3669 (2024).
14. Ghosh, S., Roy, S., Naskar, J. & Kole, R. K. Process optimization for biosynthesis of mono and bimetallic alloy nanoparticle catalysts for degradation of dyes in individual and ternary mixture. *Sci. Rep.* **10**, 277 (2020).
15. Zulfiqar, Z. et al. Plant-mediated green synthesis of silver nanoparticles: synthesis, characterization, biological applications, and toxicological considerations: a review. *Biocatal. Agric. Biotechnol.* **57**, 103121 (2024).
16. Ghosh, S., Roy, S., Naskar, J. & Kole, R. K. Plant-mediated synthesis of Mono- and bimetallic (Au–Ag) nanoparticles: future prospects for Food Quality and Safety. *J. Nanomaterials*. **2023**, 1–18 (2023).
17. Majumdar, R. & Kar, P. K. Biosynthesis, characterization and anthelmintic activity of silver nanoparticles of Clerodendrum infortunatum isolate. *Sci. Rep.* **13**, 7415 (2023).
18. Wang, J. H., Luan, F., He, X. D., Wang, Y. & Li, M. X. Traditional uses and pharmacological properties of Clerodendrum phytochemicals. *J. Tradit. Complement. Med.* **8**, 24–38 (2018).
19. Khan, S. A., Noreen, F., Kanwal, S., Iqbal, A. & Hussain, G. Green synthesis of ZnO and Cu-doped ZnO nanoparticles from leaf extracts of Abutilon indicum, Clerodendrum Infortunatum, Clerodendrum inerme and investigation of their biological and photocatalytic activities. *Mater. Sci. Eng. C.* **82**, 46–59 (2018).
20. Roy, S., Das, T. K., Maiti, G. P. & Basu, U. Microbial biosynthesis of nontoxic gold nanoparticles. *Mater. Sci. Eng. B.* **203**, 41–51 (2016).
21. Paul, T. K. et al. Mapping the progress in surface plasmon resonance analysis of phytogenic silver nanoparticles with colorimetric sensing applications. *Chem. Biodivers.* **20**, (2023).
22. Hang, Y., Wang, A. & Wu, N. Plasmonic silver and gold nanoparticles: shape- and structure-modulated plasmonic functionality for point-of-caring sensing, bio-imaging and medical therapy. *Chem. Soc. Rev.* **53**, 2932–2971 (2024).
23. Horne, J. et al. Optimization of silver nanoparticles synthesis by chemical reduction to enhance SERS quantitative performances: early characterization using the quality by design approach. *J. Pharm. Biomed. Anal.* **233**, 115475 (2023).
24. Ramos, R. M. C. R. & Regulacio, M. D. Controllable synthesis of bimetallic nanostructures using biogenic reagents: a green perspective. *ACS Omega*. **6**, 7212–7228 (2021).
25. Akintelu, S. A., Bo, Y. & Folorunso, A. S. A review on synthesis, optimization, mechanism, characterization, and antibacterial application of silver nanoparticles synthesized from plants. *J. Chem.* **2020**, 1–12 (2020).

26. Lunardi, C. N., Gomes, A. J., Rocha, F. S., De Tommaso, J. & Patience, G. S. Experimental methods in chemical engineering: Zeta potential. *Can. J. Chem. Eng.* **99**, 627–639 (2021).
27. Kamble, S. et al. Revisiting zeta potential, the key feature of interfacial phenomena, with applications and recent advancements. *ChemistrySelect* **7**, (2022).
28. Millour, M. et al. Effects of concentration and chemical composition of natural organic matter on the aggregative behavior of silver nanoparticles. *Colloids Surf. A*. **623**, 126767 (2021).
29. Riaz, M. et al. Exceptional antibacterial and cytotoxic potency of monodisperse greener AgNPs prepared under optimized pH and temperature. *Sci. Rep.* **11**, (2021).
30. Biomolecule-assisted biogenic. Synthesis of metallic nanoparticles. In *Agri-Waste and Microbes for Production of Sustainable Nanomaterials* 139–163. https://doi.org/10.1016/b978-0-12-823575-1.00011-1. (Elsevier, 2022).
31. Hadi, A. A., Ng, J. Y., Shamsuddin, M., Matmin, J. & Malek, N. A. N. N. Green synthesis of silver nanoparticles using Diplazium esculentum extract: catalytic reduction of methylene blue and antibacterial activities. *Chem. Pap*. **76**, 65–77 (2022).
32. Ahani, M. & Khatibzadeh, M. Green synthesis of silver nanoparticles using gallic acid as reducing and capping agent: effect of pH and gallic acid concentration on average particle size and stability. *Inorg. Nano-Metal Chem.* **52**, 234–240 (2022).
33. Tsegay, M. G., Gebretinsae, H. G., Sackey, J., Maaza, M. & Nuru, Z. Y. Green synthesis of khat mediated silver nanoparticles for efficient detection of mercury ions. *Materi. Today Proc.* **36**, 368–373 (2021).
34. Tew, W. Y. et al. Application of FT-IR spectroscopy and chemometric technique for the identification of three different parts of Camellia Nitidissima and discrimination of its authenticated product. *Front. Pharmacol.* **13**, 931203 (2022).
35. Coates, J. Interpretation of infrared spectra, a practical approach. In *Encyclopedia of Analytical Chemistry* (ed. Meyers, R. A.) https://doi.org/10.1002/9780470027318.a5606 (Wiley, 2000).
36. Maniraj, A., Kannan, M., Rajarathinam, K., Vivekanandhan, S. & Muthuramkumar, S. Green synthesis of silver nanoparticles and their effective utilization in fabricating functional surface for antibacterial activity against multi-drug resistant Proteus mirabilis. *J. Clust Sci.* **30**, 1403–1414 (2019).
37. Garibo, D. et al. Green synthesis of silver nanoparticles using Lysiloma acapulcensis exhibit high-antimicrobial activity. *Sci. Rep.* **10**, 12805 (2020).
38. Sharma, N. K. et al. Green route synthesis and characterization techniques of silver nanoparticles and their biological adeptness. *ACS Omega*. **7**, 27004–27020 (2022).
39. Iqbal, N. et al. Environmentally benign design of renewable oleoresin-bioenergized imidacloprid nanohydrocolloids for improved activity, lower toxicity, and agroecological sustainability. *ACS Sustain. Chem. Eng.* **11**, 15480–15491 (2023).
40. Dutta, S. D. P. Comparative phytochemical profiling of *Clerodendrum infortunatum* L. using GC-MS method coupled with multivariate statistical approaches. *Metabolomics* 05, (2015).
41. Dutta, S. et al. Stimulation of murine immune response by Clerodendrum Infortunatum. *Phcog Mag.* **14**, 417 (2018).
42. Khatun, M. S. et al. Evaluation of anti-inflammatory potential and GC-MS profiling of leaf extracts from *Clerodendrum infortunatum* L. *J. Ethnopharmacol.* **320**, 117366 (2024).
43. Akhil, B. S. et al. Exploring the Phytochemical Profile and Biological activities of *Clerodendrum Infortunatum*. *ACS Omega*. **8**, 10383–10396 (2023).
44. Dash, S. S., Samanta, S., Dey, S., Giri, B. & Dash, S. K. Rapid Green Synthesis of Biogenic Silver nanoparticles using *Cinnamomum tamala* Leaf Extract and its potential antimicrobial application against clinically isolated Multidrug-resistant bacterial strains. *Biol. Trace Elem. Res.* **198**, 681–696 (2020).
45. Razavi, M. et al. Green chemical and biological synthesis of nanoparticles and their biomedical applications. In *Green Processes for Nanotechnology* (eds Basiuk, V. A. & Basiuk, E. V.) 207–235. https://doi.org/10.1007/978-3-319-15461-9_7. ((Springer International Publishing, 2015).
46. Labulo, A. H., David, O. A. & Terna, A. D. Green synthesis and characterization of silver nanoparticles using *Morinda lucida* leaf extract and evaluation of its antioxidant and antimicrobial activity. *Chem. Pap*. **76**, 7313–7325 (2022).
47. Jain, S. & Mehata, M. S. Medicinal plant leaf extract and pure flavonoid mediated green synthesis of silver nanoparticles and their enhanced antibacterial property. *Sci. Rep.* **7**, 15867 (2017).
48. Tarannum, N., Divya, D. & Gautam, Y. K. Facile green synthesis and applications of silver nanoparticles: a state-of-the-art review. *RSC Adv.* **9**, 34926–34948 (2019).
49. Gupta, A. et al. Trimetallic composite nanofibers for antibacterial and photocatalytic dye degradation of mixed dye water. *Appl. Nanosci.* **10**, 4191–4205 (2020).
50. Kumar Mandal, R., Ghosh, S. & Pal Majumder, T. Comparative study between degradation of dyes (MB, MO) in monotonous and binary solution employing synthesized bimetallic (Fe-CdO) NPs having antioxidant property. *Results Chem.* **5**, 100788 (2023).
51. Mandal, R. K., Mondal, A. S., Ghosh, S., Halder, A. & Majumder, T. P. Synthesis, characterisation and optical studies of CdO-NiO NCs for comparative dye degradation study between two hazardous dyes Congo Red and Rose Bengal. *Results Chem.* **5**, 100810 (2023).
52. Ajibade, P. A. & Oluwalana, A. E. Enhanced photocatalytic degradation of ternary dyes by copper sulfide nanoparticles. *Nanomaterials* **11**, 2000 (2021).
53. Basavaraj, N., Sekar, A. & Yadav, R. Review on green carbon dot-based materials for the photocatalytic degradation of dyes: fundamentals and future perspective. *Mater. Adv.* **2**, 7559–7582 (2021).
54. Kumari, H. et al. A review on photocatalysis used for wastewater treatment: dye degradation. *Water Air Soil. Pollut.* **234**, 349 (2023).
55. Lazaar, K. et al. Effective decoloration of cationic dyes by silica gel prepared from Tunisian sands and TiO2/silica gel composites: dual adsorption and photocatalytic processes. *Desalin. Water Treat.* **179**, 368–377 (2020).
56. Agnihotri, S., Sillu, D., Sharma, G. & Arya, R. K. Photocatalytic and antibacterial potential of silver nanoparticles derived from pineapple waste: process optimization and modeling kinetics for dye removal. *Appl. Nanosci.* **8**, 2077–2092 (2018).
57. Kiwaan, H. A., Atwee, T. M., Azab, E. A. & El-Bindary, A. A. Photocatalytic degradation of organic dyes in the presence of nanostructured titanium dioxide. *J. Mol. Struct.* **1200**, 127115 (2020).
58. Selvaraj, V., Karthika, S., Mansiya, T., Alagar, M. & C. & An over review on recently developed techniques, mechanisms and intermediate involved in the advanced azo dye degradation for industrial applications. *J. Mol. Struct.* **1224**, 129195 (2021).
59. Bibi, F. et al. Impact of Co and Cu co-doping on the structural, electrical, magnetic and solar light driven photo-catalytic properties of $NiFe_2O_4$ nano-crystals for crystal violet dye removal. *ChemistrySelect* **9**, e202400372 (2024).
60. Priyadarshini, S. S., Sethi, S., Rout, S., Mishra, P. M. & Pradhan, N. Green synthesis of microalgal biomass-silver nanoparticle composite showing antimicrobial activity and heterogenous catalysis of nitrophenol reduction. *Biomass Convers. Bioref.*. **13**, 7783–7795 (2023).
61. Mondal, K. & Sharma, A. Recent advances in the synthesis and application of photocatalytic metal–metal oxide core–shell nanoparticles for environmental remediation and their recycling process. *RSC Adv.* **6**, 83589–83612 (2016).
62. Shabil Sha, M. et al. Photocatalytic degradation of organic dyes using reduced graphene oxide (rGO). *Sci. Rep.* **14**, 3608 (2024).
63. Khan, Z. U. H. et al. Biomedical and photocatalytic applications of biosynthesized silver nanoparticles: Ecotoxicology study of brilliant green dye and its mechanistic degradation pathways. *J. Mol. Liq.* **319**, 114114 (2020).
64. Nawaz, A. et al. Synthesis of ternary-based visible light nano-photocatalyst for decontamination of organic dyes-loaded wastewater. *Chemosphere* **289**, 133121 (2022).

65. Saeed, M., Muneer, M., Haq, A. U. & Akram, N. Photocatalysis: an effective tool for photodegradation of dyes—a review. *Environ. Sci. Pollut. Res.* **29**, 293–311 (2022).
66. Khan, S., Noor, T., Iqbal, N. & Yaqoob, L. Photocatalytic dye degradation from textile wastewater: a review. *ACS Omega*. **9**, 21751–21767 (2024).
67. Khan, I. et al. Heterogeneous photodegradation of industrial dyes: an insight to different mechanisms and rate affecting parameters. *J. Environ. Chem. Eng.* **8**, 104364 (2020).
68. Koe, W. S., Lee, J. W., Chong, W. C., Pang, Y. L. & Sim, L. C. An overview of photocatalytic degradation: photocatalysts, mechanisms, and development of photocatalytic membrane. *Environ. Sci. Pollut. Res.* **27**, 2522–2565 (2020).
69. Kalaycıoğlu, Z., Özuğur Uysal, B., Pekcan, Ö. & Erim, F. B. Efficient photocatalytic degradation of methylene blue dye from aqueous solution with cerium oxide nanoparticles and graphene oxide-doped polyacrylamide. *ACS Omega*. **8**, 13004–13015 (2023).
70. Asefa, G., Negussa, D., Lemessa, G. & Alemu, T. The study of photocatalytic degradation kinetics and mechanism of malachite green dye on Ni–TiO2 surface modified with polyaniline. *J. Nanomater.*. **2024**, 1–11 (2024).
71. Rani, G., Bala, A., Ahlawat, R., Nunach, A. & Chahar, S. Recent advances in synthesis of AgNPs and their role in degradation of Organic dyes. *Comments Inorg. Chem.* 1–29 https://doi.org/10.1080/02603594.2024.2312394 (2024).
72. Ghaffar, S. et al. Construction of visible-light-induced Fe2O3/g-C3N4 nanocomposites for the enhanced degradation of organic dyes: optimization of operative parameters. *Polyhedron* **264**, 117254 (2024).
73. Ahmed, A. et al. Synthesis of visible-light-responsive lanthanum-doped copper ferrite/graphitic carbon nitride composites for the photocatalytic degradation of toxic organic pollutants. *Diam. Relat. Mater.* **141**, 110630 (2024).
74. Ahmed, D. et al. Efficient degradation of atrazine from synthetic water through photocatalytic activity supported by titanium dioxide nanoparticles. *Z. fÃ¼r Phys. Chem.* **237**, 395–412 (2023).
75. Mohamadpour, F. & Amani, A. M. Photocatalytic systems: reactions, mechanism, and applications. *RSC Adv.* **14**, 20609–20645 (2024).
76. Naraginti, S. & Li, Y. Preliminary investigation of catalytic, antioxidant, anticancer and bactericidal activity of green synthesized silver and gold nanoparticles using *Actinidia deliciosa*. *J. Photochem. Photobiol. B.* **170**, 225–234 (2017).
77. Elbadawy, H. A., Elhusseiny, A. F., Hussein, S. M. & Sadik, W. A. Sustainable and energy-efficient photocatalytic degradation of textile dye assisted by ecofriendly synthesized silver nanoparticles. *Sci. Rep.* **13**, 2302 (2023).
78. Usman, M. et al. Unveiling the synthesis of magnetically separable magnetite nanoparticles anchored over reduced graphene oxide for enhanced visible-light-driven photocatalytic degradation of dyes. *Diam. Relat. Mater.* **149**, 111575 (2024).
79. Haqmal, E., Senthil, R. A., Ahmed, A. & Pan, J. Uncovering the influence of Ni-doping in CuBi2O4 photocatalyst on its visible-light-responsiveness for the efficient removal of toxic alizarin yellow R dye from wastewater. *Colloids Surf. A*. **684**, 133185 (2024).
80. Naraginti, S., Li, Y. & Puma, G. L. Photocatalytic mineralization and degradation kinetics of sulphamethoxazole and reactive red 194 over silver-zirconium co-doped titanium dioxide: reaction mechanisms and phytotoxicity assessment. *Ecotoxicol. Environ. Saf.* **159**, 301–309 (2018).
81. Gunture et al. Pollutant diesel soot derived onion-like nanocarbons for the adsorption of organic dyes and environmental assessment of treated wastewater. *Ind. Eng. Chem. Res.* **59**, 12065–12074 (2020).
82. Naraginti, S., Li, Y., Wu, Y., Zhang, C. & Upreti, A. R. Mechanistic study of visible light driven photocatalytic degradation of EDC 17α-ethinyl estradiol and azo dye Acid Black-52: phytotoxicity assessment of intermediates. *RSC Adv.* **6**, 87246–87257 (2016).
83. Chatterjee, K., Banoo, M., Mondal, S., Sahoo, L. & Gautam, U. K. Synthesis of Bi_3TaO_7–Bi_4TaO_8 br composites in ambient air and their high photocatalytic activity upon metal loading. *Dalton Trans.* **48**, 7110–7116 (2019).
84. Ghosh, S. et al. Ecological safety with multifunctional applications of biogenic mono and bimetallic (Au–Ag) alloy nanoparticles. *Chemosphere* **288**, 132585 (2022).

Acknowledgements

The authors greatly appreciate Prof. Ramen Kumar Kole, Export Testing Laboratory (ETL), Dept. of Ag-Chemicals, BCKV, WB, India for providing the essential instrumental and infrastructural facilities. The zeta potential measurements, DLS, and other analyses were made possible by Prof. T. Basu and Dr. Jishu Naskar of the Dept. of Biochemistry and Biophysics at the University of Kalyani, WB, India, which the authors sincerely thank for their help. We also acknowledge the recording of the IR spectra by the Department of Chemistry, University of Kalyani, WB, India. The authors are grateful to Central National Herbarium (CAL), Botanical Survey of India for the correct identification of the plant species and also thankful to Mr. Tanay Shil, Senior Preservation Assistant, Central National Herbarium, Botanical Survey of India for helping in our work. The authors were sincerely thankful to the Department of Botany, Kalna College (Purba Bardhaman, WB, India) for allowing the depositing of plant material (voucher specimen).

Author contributions

K.M., D.D., S.G., assisted in the experiments; S.K.B., A.C., A.C., S.M., S.G. contributed to the literature review and calculation; S.G., S.R. designed and supervised the experiments, wrote the original draft, and reviewed the manuscript. All the authors have read and approved the final version of the manuscript.

Declarations

Competing interests

The authors declare no competing interests.

Additional information

Supplementary Information The online version contains supplementary material available at https://doi.org/10.1038/s41598-024-82341-7.

Correspondence and requests for materials should be addressed to S.G. or S.R.